Strong Interlayer Magnon-Magnon Coupling in Magnetic Metal-Insulator Hybrid Nanostructures

Jilei Chen, Chuanpu Liu, Tao Liu, Yang Xiao, Ke Xia, Gerrit E. W. Bauer, Mingzhong Wu, and Haiming Yu

Phys. Rev. Lett. **120**, 217202 — Published 23 May 2018

DOI: 10.1103/PhysRevLett.120.217202

Strong interlayer magnon-magnon coupling in magnetic metal/insulator hybrid nanostructures

Jilei Chen,[1,*] Chuanpu Liu,[1,*] Tao Liu,[2,*] Yang Xiao,[3,*] Ke Xia,[4]
Gerrit E. W. Bauer,[5,6] Mingzhong Wu,[2] and Haiming Yu[1,†]

[1] *Fert Beijing Institute, BDBC, School of Electronic and Information Engineering, Beihang University, Xueyuan Road 37, Beijing 100191, China*
[2] *Department of Physics, Colorado State University, Fort Collins, Colorado 80523, USA*
[3] *Department of Applied Physics, Nanjing University of Aeronautics and Astronautics, Nanjing 210016, China*
[4] *Department of Physics, Beijing Normal University, Beijing 100875, China*
[5] *Institute for Materials Research, WPI-AIMR and CSNR, Tohoku University, Sendai 980-8577, Japan*
[6] *Zernike Institute for Advanced Materials, University of Groningen, Nijenborgh 4, 9747 AG Groningen, The Netherlands*

We observe strong interlayer magnon-magnon coupling in an on-chip nanomagnonic device at room temperature. Ferromagnetic nanowire arrays are integrated on a 20-nm-thick yttrium iron garnet (YIG) thin film strip. Large anticrossing gaps up to 1.58 GHz are observed between the ferromagnetic resonance of the nanowires and the in-plane standing spin waves of the YIG film. Control experiments and simulations reveal that both the interlayer exchange coupling and the dynamical dipolar coupling contribute to the observed anticrossings. The coupling strength is tunable by the magnetic configuration, allowing coherent control of magnonic devices.

Strong couplings between photons and spins, atoms and superconducting qubits lie at the heart of realizing the quantum manipulation in quantum dots, nitrogen-vacancy centers and mechanical oscillators [1–5]. Cavity magnon polaritons [6–12], i.e. the hybrid state of a cavity photon and a spin wave excitation in a magnet in the cavity, have been evidence of such coupling at both ultralow and room temperatures. Strong couplings have been observed in sub-millimeter-sized yttrium iron garnet (YIG) spheres [10–12], which obeyed the size scaling law proposed by R. H. Dicke [13], i.e. $g \propto \sqrt{N}$ with N the number of spins. However, Dicke's law implies weak couplings when magnets become small in nanomagnonic devices [14–22], disqualifying microwaves for coherent control at the nanoscale.

Here, we report realization of strong coupling of magnons not in photonic, but magnonic cavities with standing magnon modes. This is analog to the magnon polariton but the cavity mode is magnonic rather than photonic, and it happens on a smaller length scale. We observe anticrossing gaps as large as 1.58 GHz at a frequency of about 7.5 GHz in heterostructures consisting of a metallic ferromagnet wire array on top of a thin-film magnetic insulator YIG. This large anticrossing gap approaches the ultrastrong coupling regime, comparable to what is observed for macroscopic cavity magnon polaritons [11]. We can control the coupling by the magnetization alignments, analogous to the tunable band gaps of magnonic crystals [23–30] that would be difficult to realize in photonic devices. The strong coupling between spatially separated nanomagnets offers new functionalities towards magnon transistors [31] or spin-wave logic [32].

A schematic of the nanomagnonic device is shown in Fig. 1(a). YIG thin films with thickness $t_1 = 20$ nm were grown on $Gd_3Ga_5O_{12}$ (GGG) substrates by magnetron sputtering and patterned by ion beam etching (IBE) to form a magnon waveguide of 90 μm width. Magnetic nanowire arrays were deposited on top of a YIG waveguide by electron beam evaporation with thickness of t_2 (20 nm thick nickel or 30 nm thick cobalt) [33]. a stands for the center-to-center distance of two neighbouring nanowires, i.e. the period of the array. A scanning electron microscope (SEM) image of the nanomagnonic arrays with $a = 600$ nm is shown in Fig. 1(b). An external magnetic field was applied (initially) parallel to the nanowires. We excite and detect spin waves using coplanar waveguides (CPWs) integrated on top of the nanowire arrays. The scattering parameter S_{11} for reflection is measured by a vector network analyzer

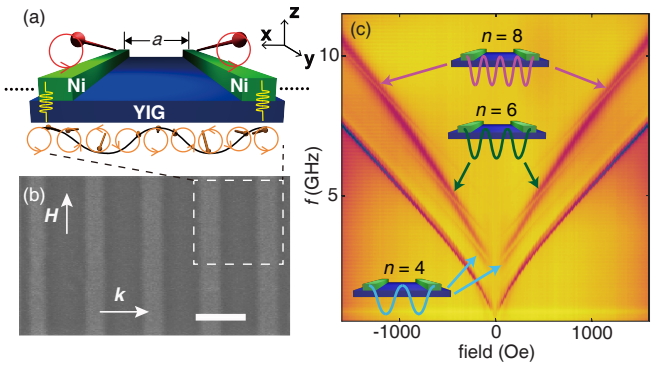

FIG. 1. (a) Sketch of a hybrid magnetic nanostructure based on a YIG thin film. The applied field H is in-plane and parallel to the nanowires. (b) An SEM image (scale bar 500 nm) of the Ni-based nanowire array on YIG thin film. (c) Color-coded reflection spectra S_{11} measured on the Ni/YIG hybrid nanostructures by a coplanar waveguide. The arrows highlight anticrossing modes induced by different in-plane standing spin wave modes with mode numbers $n = 4, 6, 8$.

(VNA) connected to the CPW (Fig. S1) [33, 36–39]. The nanowire arrays on top of the YIG thin film act as Bragg scattering gratings to form in-plane standing spin waves (iSSWs) with large wave numbers as illustrated in Fig. 1(a).

Figure 1(c) shows reflection spectra S_{11} measured as a function of frequency and magnetic field where two main branches are observed. The lower-frequency branches agree with the spin-wave resonance of a bare YIG film in the Damon-Eshbach (DE) configuration [38], whereas those at higher frequencies are assigned to the ferromagnetic resonance (FMR) of the Ni wires. The Ni modes can be fitted with an in-plane demagnetization factor $N_{xx} = 0.01$ [27]. This value is smaller than the expected form factor of a wire, which has been reported also by Ding et al. [40]. Dipolar interactions at the edges [41] or between neighbouring wires could explain the observed reduction of the anisotropy. Here we focus on the three pronounced anticrossings (marked with arrows) observed in the Ni resonances that we attribute to the interlayer coupling between the FMR of Ni and high-order iSSWs in YIG as sketched in Fig. 1(a).

Spin waves in a periodic potential develop a band structure with gaps at the Brillouin zone boundaries with wavenumber π/a, where a is the unit cell length. In the limit of a strong periodic potential, the superlattice band structure becomes dispersionless, the spin waves are all localized in each unit cell, and the band index n counts the number of nodes. When the frequency of a standing spin wave in YIG approaches a resonance of the Ni wire array, a coupling results in a level repulsion or anticrossing (see Fig. 2(a)). When the nanowires are at resonance, the strong magnetization of the relatively hard magnetic material Ni drives a spin precession in the relatively soft magnetic YIG through interlayer magnetic coupling. Since the FMR of Ni ensures in-phase precession in all nanowires, the YIG film beneath each nanowire precesses in-phase as well. The associated dynamic periodic boundary conditions can be fulfilled by in-plane standing spin waves for even number of nodes only ($n = 2$, 4, 6). In contrast, only odd-numbered perpendicular standing spin waves (PSSWs) are observed in the spin wave resonance of intrinsic thin films [42] when there is surface pinning of the magnetization, which is not so important in the present transverse geometry. The three observed anticrossing modes in Fig. 1(c) can be fitted by dipolar-exchange spin wave dispersion relations of YIG film [43] taking exchange constant $\lambda_{\rm ex} = 3 \times 10^{-16}$ m^2 [44], the saturation magnetization $4\pi M_{\rm S} = 1766$ G [20], film thickness being 20 nm and $k = n\pi/a$. As a result, these three modes are attributed to iSSWs with mode numbers $n = 4$, $n = 6$ and $n = 8$. Schematic drawings of these three high-order iSSWs are shown in the insets of Fig. 1(c). The PSSWs of the YIG films resonate at frequencies > 35 GHz and are not relevant for the present study.

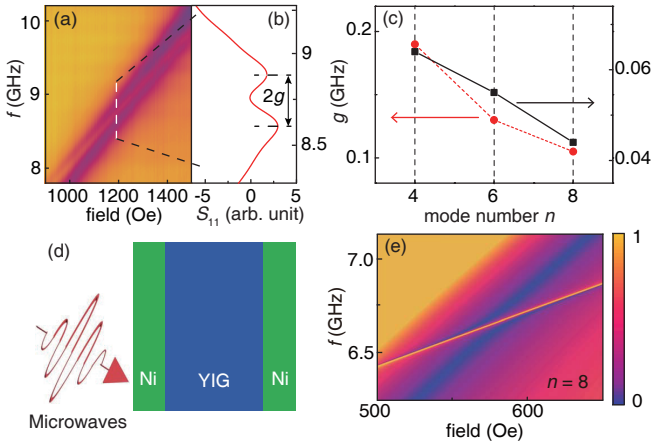

FIG. 2. (a) Color-coded reflection spectra S_{11} for high-order iSSWs with mode number of $n = 8$. (b) The line spectrum selects the spectrum indicated by the vertical dotted line in (a) at 1200 Oe. The frequency gap in the anticrossing mode reveals the coupling strength g. (c) g as a function of the mode number $n = 4$, 6 and 8. Red dots: experiments. Black squares: simulations. (d) Schematic of the modelled structure. The width of YIG and Ni are 500 nm and 100 nm, respectively. (b) Simulation results of reflection spectra as a function of in-plane magnetic field for the anticrossing of Ni FMR mode and $n = 8$ iSSW YIG mode. The color represents the reflection amplitude with scale definition on the side.

In Fig. 2(a) and (b), an anticrossing gap of 120 MHz is observed for the $n = 8$ mode. The anticrossing covers a broad frequency range because the Ni FMR mode and the $n = 8$ iSSW mode run nearly parallel. The coupling strength g is defined as half of the minimal peak-to-peak frequency spacing in the anticrossing. The coupling strengths g extracted for all three anticrossings are plotted in Fig. 2(c). For spin wave resonance of films with thickness d and pinned surface magnetization [8, 33], the coupling strength decreases as $g^{(n)} \propto \sqrt{d}/n$, where n is a PSSW mode number. In our case, the driving force is not the homogeneous ac field but the localized field beneath Ni nanowires. Nevertheless, with increasing n the overlap with the applied ac magnetic field is increasingly averaged out, leading to a $g \propto 1/n$ scaling as in conventional spin wave resonance [8, 33, 42]. We can also extract a dissipation rate for $n = 8$ in terms of the half-width at half maximum of the line broadenings as $\kappa_m^{\rm Ni} \approx 0.63$ GHz and $\kappa_m^{\rm YIG} \approx 0.06$ GHz. This fulfills the condition for a magnetically induced transparency (MIT) [11] for magnon transmission, since $\kappa_m^{\rm Ni} > g > \kappa_{\rm m}^{\rm YIG}$. The magnon-magnon cooperativity

$$C = g^2/(\kappa_{\rm m}^{\rm Co} \times \kappa_{\rm m}^{\rm YIG}) \qquad (1)$$

is large, $C = 0.38$ in our case. Returning to the analogy with magnon polaritons, we note that the YIG magnons play the role of the cavity photons, while the Ni wire array forms the scattering object. We do not observe the

scattering properties of YIG magnons directly, but rather use the (auxiliary) microwave photons in order to study the coupled system. The anticrossing is caused by the periodic driving forces under the nickel FMR. Magnetization dynamics is studied in a Permalloy/YIG system by spin pumping effect not reporting anticrossing phenomena [48].

Results of model calculations of microwave absorption spectra of Ni/YIG magnetic hybrid nanostructures are shown in Fig. 2(e) for $n = 8$ mode as an example (full simulation results are shown in Fig. S3). We consider a thin-film trilayer Ni/YIG/Ni with magnetic field driven by microwaves as shown in Fig. 2(d). This structure is a simplification of the experimental situation, but captures the salient features of the observations. The PSSWs in this 1-D geometry correspond to the iSSWs in the experimental structure. The reflection spectrum S_{11} shown in Fig. 2(e) is calculated by the transfer matrix method that involves solving the coupled Maxwell and Landau-Lifshitz-Gilbert (LLG) equations. The SSWs are governed by magnetization boundary conditions that we chose here to be partially free (Fig. S2) [49]:

$$A\frac{\partial m_{1z}}{\partial z} - K_s m_{1z} + A_{12}\frac{M_1}{M_2}m_{2z} = 0 \qquad (2)$$

with m_{nz}, M_n, A, A_{12} and K_s being the out-of-plane component of the dynamic magnetization, saturation magnetization, exchange stiffness, interlayer exchange interaction with its neighbouring layer and interface uniaxial anisotropy field, respectively. z axis is normal to the multilayers. In Fig. 2(e), we chose an interlayer exchange coupling between Ni and YIG of $A_{12} = 0.03$ erg/cm^2, which couples the SSWs of YIG and FMR mode of Ni. The anticrossing gaps in Fig. 2(c) decrease with increasing SSW mode number n since higher order SSWs have smaller dynamical magnetization amplitudes at the interface. The detailed analysis on the dependence of anticrossing gap on the multilayer structure, spin wave order and coupling mechanism will be given in a separate paper [50]. By tuning the parameters, e.g. A, A_{12} and K_s, we find that the interlayer exchange coupling contributes to the anticrossing gap. The ferromagnetic interfacial exchange coupling in thicker YIG/ferromagnet extended bilayers has been confirmed experimentally [51–54]. For higher-order SSW modes, the interaction between SSW and FMR becomes weaker as observed (see Fig. 2(c)).

We now change the material of the nanowire array to a harder magnet (cobalt) and scale down the nanowire periodicity to 180 nm. In these samples we measured the full spectra from -1000 Oe to 1000 Oe [33]. The coupling strength can be controlled by varying the magnetic alignments between YIG and Co wires. Sweeping the external magnetic field gives rise to three different types of magnetization textures that characteristically modulates the reflection spectra S_{11} as shown in Fig. 3. The higher FMR frequency is caused by the larger saturation magnetization of Co compared with Ni. Figure 3(a) shows the S_{11} spectra when magnetizations of YIG and Co are parallel (denoted as "P" state). A lineplot for -450 Oe is shown in Fig. 3(b). An anticrossing appears when the Co FMR mode crosses with the $n = 4$ iSSW YIG mode. Figure 3(c) shows the extracted maxima of the resonances as well as calculated Co and YIG modes following Ref. [44]. The coupling strength g is 284 MHz. The coupling strength can be varied by the nanowire widths [33]. Compared with the Ni-based structure, the coupling strength is slightly enhanced. Nevertheless, taking into account broadening of the Co resonance, the system is still in the MIT regime [11].

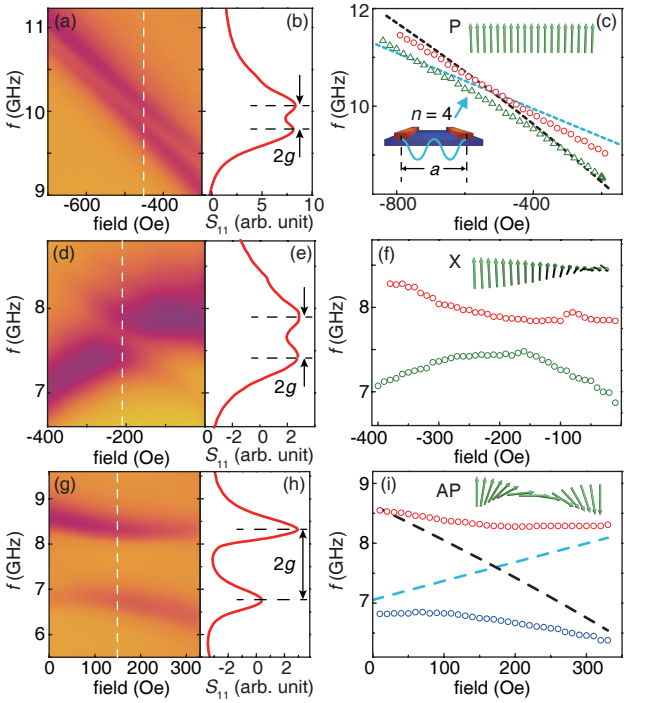

FIG. 3. (a) Color-coded reflection spectra S_{11} for $n = 4$ iSSW mode. (b) The line spectrum is extracted at -450 Oe. (c) Data points extracted from experimental data by reading out the maxima of each resonances. The insets depict the $n = 4$ iSSW mode and the parallel state of Co/YIG multilayer. Black dashed line: Co FMR mode. Blue dotted lines: $n = 4$ iSSW modes of YIG thin film. (a) to (c) are data for P states. (d) to (f) present data for X state. (g) to (i) present data for AP state of Co/YIG hybrids. [33] All data presented in this figure are data from $n = 4$ iSSW mode.

The situation changes when the magnetization becomes noncollinear. With a small external field perpendicular to the Co nanowires, their magnetizations remain along wire axis due to a large demagnetization field [40], but the magnetization of the soft YIG layer is rotated. The size of the anticrossing gap of this magnetic configuration (denoted as "X" state) in Fig. 3(d-e) is much larger than that of the P state. Furthermore, as shown in Fig. 3(g-i), an increased magnetic field along

the nanowires can even bring the YIG/Co bilayer into an antiparallel state (marked by "AP"). The full spectra of P, X and AP states are presented in Figs. S4-S5 [33]. The AP state exhibits a remarkably large anticrossing gap up to 1.58 GHz. One can extract from experiments $\kappa_{\rm m}^{\rm Co} \approx 0.50$ GHz and $\kappa_{\rm m}^{\rm YIG} \approx 0.06$ GHz away from the anticrossing. This indicates a strong coupling is formed where $g > \kappa_{\rm m}^{\rm Co}$ and $g > \kappa_{\rm m}^{\rm YIG}$ [11]. We can calculate a cooperativity $C = 21$! Considering the resonance frequency $\omega_{\rm a} \approx 7.5$ GHz, the coupled system yields a ratio of $g/\omega_{\rm a} = 10.5\%$ that reaches the ultrastrong coupling (USC) regime (the highest USC coupling ratio achieved in Ref. [11] is 6.7%).

The USC may be attributed to the enhanced interlayer coupling strength arising from the exchange spring effect. Essential for the nanofabrication is a 1 nm-thick Ti layer between YIG and the Co/Ni nanowires that acts as an adhesive during lift-off. The Ti layer should be thin enough to ensure a ferromagnetic-type interlayer exchange coupling [45]. In the P configuration, there should be no texture since the interlayer exchange favours P state. As we rotate the magnetization of one of the two magnetic layers while the magnets remain collinear at the interface, we create an exchange spring near the interface that penetrates into the YIG layer over the exchange length that can be large for soft magnetic materials.

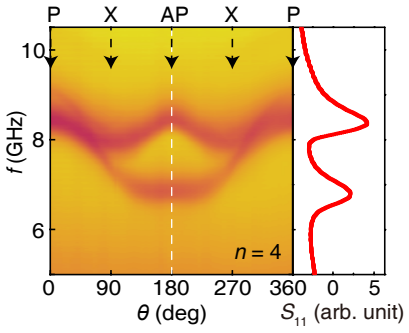

FIG. 4. Angle dependent microwave spectra. θ is the in-plane magnetic field angle with respect to the orientation of the nanowires. At the applied field of 170 Oe the Co wire magnetization is not modified and the YIG magnetization is nearly parallel with the field direction. So 0° corresponds to the P and 180° the AP state. The splitting of the lines is the anticrossing between the $n = 4$ iSSW mode and the Co FMR. A lineplot at 180° is shown as an example of color-vs-intensity code.

The angle dependent measurements in Fig. 4 are additional evidence for the lateral "exchange spring". The ferromagnetic interlayer exchange coupling twists the magnetization with increasing angle. The exchange spring is twisted by 180 degrees in the AP configuration. The perturbation of the surface spin waves in YIG by the Co wires is then maximizes, generating large anticrossing gap. Between each step of the angular dependence measurements the magnetic field is switched off and on in order to suppress non-universal effects due to the sweep history. As a consequence the spectra in Fig. 4 are symmetric about the 180 degrees angle. The observed collapse of the gap when reducing the magnetic field angle can be understood by the corresponding relaxation of the spring. While we are not able to observe the magnetic texture directly with our technique, this is strong evidence for an interface exchange controlled surface magnetization. A "re-open" of the gap at 0 deg is observed which is possibly due to the fact that at P state 170 Oe is off the crossing point (around 450 Oe, see Fig. 3(a-c)), and therefore these two modes become separated Co and YIG modes. Such strong angular dependance may also be related to 1D bicomponent magnonic crystal band structure [46].

Notably, the residual mode splitting observed in the sample with thin alumina barrier (Fig. S7) reflects a contribution from the dynamical dipolar coupling [47]. The resonance in the ferromagnetic nanowires generates oscillating magnetic charges whose stray fields interact with the YIG magnetization. The amplitude of the dynamical dipolar coupling can be estimated as $\frac{1}{2}N_{xx}\gamma 4\pi M_{\rm s}$ [55], which amounts to 0.83 GHz for the sample in Fig. 4. This value is not negligible compared to the interlayer exchange coupling. More precise estimations require detailed micromagnetic modelling beyond the scope of the present paper, however.

In conclusion, we demonstrate an anticrossing between the magnon modes in ferromagnetic nanowires and the substrate formed by a magnetic insulator YIG thin film. The measured spectra prove that the FMR modes of ferromagnetic nanowires couple with high-order iSSW modes in YIG films. The coupling strength is tunable over a large range by varying the magnetization alignment of the nanowires and films. Simulations and control experiments indicate that both interlayer exchange and dynamical dipolar couplings contribute to the observed splittings. The comparison of Ni/YIG and Co/YIG hybrid nanostructures suggests that material engineering of nanomagnonic devices can enhance their functionalities.

The authors thank J. Hu, W. Zhao, Z.M. Liao and D.P. Yu for sample fabrications and S. Tu, T. Stückler, F. Heimbach, Y. Cao, Y. Zhang, S. Granville and B.A. Kalinikos for helpful discussions. We wish to acknowledge the support by NSF China under Grant No. 11674020, youth 1000 plan, 111 talent program B16001. KX is supported by National Key Research and Development Program of China (Grant No. 2017YFA0303304) and the National Natural Science Foundation of China (No.61774017, 11734004 and 21421003). TL and MW were supported by SHINES, an Energy Frontier Research Center funded by the U.S. Department of Energy (SC0012670), and the U.S. National Science Foundation (EFMA1641989 and DMR-1407962). GB was supported

by the Netherlands Organization for Scientific Research (NWO) and by JSPS Kakenhi (Japan) Grants-in-Aid for Scientific Research (Grant No. 26103006).

Note added.—During the review process of this manuscript, reports on anticrossings in the FMR of extended bilayers between the Co Kittel mode and perpendicular standing spin waves in a μm-thick YIG film [56] and between the CoFeB Kittel mode and perpendicular standing spin waves in a 295 nm-thick YIG film [57] have been posted.

* These authors contributed equally to this work.
† haiming.yu@buaa.edu.cn

[1] Y. Tabuchi, S. Ishino, A. Noguchi, T. Ishikawa, R. Yamazaki, K. Usami and Y. Nakamura, Science **349**, 405-408 (2015).
[2] X. Zhu, S. Shiro, A. Kemp, K. Kakuyanagi, S.-I. Karimoto, H. Nakano, W.J. Munro, Y. Tokura, M.S. Everitt, K. Nemoto, M. Kasu, N. Mizuochi and K. Semba, Nature (London) **478**, 221-224 (2011).
[3] J. Majer, J.M. Chow, J.M. Gambetta, J. Koch, B.R. Johnson, J.A. Schreier, L. Frunzio, D.I. Schuster, A.A. Houck, A. Wallraff, A. Blais, M.H. Devoret, S.M. Girvin and R.J. Schoelkopf, Nature (London) **449**, 443-447 (2007).
[4] A. Imamoglu, Phys. Rev. Lett. **102**, 083602 (2009).
[5] J.H. Wesenberg, A. Ardavan, G.A.D. Briggs, J.J.L. Morton, R.J. Schoelkopf, D.I. Schuster and K. Molmer, Phys. Rev. Lett. **103**, 070502 (2009).
[6] L. Bai, M. Harder, Y.P. Chen, X. Fan, J.Q. Xiao and C.M. Hu, Phys. Rev. Lett. **114**, 227201 (2015).
[7] H. Huebl, C.W. Zollitsch, J. Lotze, F. Hocke, M. Greifenstein, A. Marx, R. Gross and S.T.B. Goennenwein, Phys. Rev. Lett. **111**, 127003 (2013).
[8] Y. Cao, P. Yan, H. Huebl, S.T.B. Goennenwein and G.E.W. Bauer, Phys. Rev. B **91**, 094423 (2015).
[9] B.M. Yao, Y.S. Gui, Y. Xiao, H. Guo, X.S. Chen, W. Lu, C.L. Chien and C.M. Hu, Phys. Rev. B **92**, 184407 (2015).
[10] J.A. Haigh, N.J. Lambert, A.C. Doherty and A.J. Ferguson, Phys. Rev. B **91**, 104410 (2015).
[11] X. Zhang, C-L. Zou, L. Jiang and H.X. Tang, Phys. Rev. Lett. **113**, 156401 (2014).
[12] X. Zhang, C-L. Zou, Zhu, N., Marquardt, F., Jiang, L. and H.X. Tang, Nat. Commun. **6**, 18 (2015).
[13] R.H. Dicke, Phys. Rev. **93**, 99-110 (1954).
[14] A.V. Chumak, V.I. Vasyuchka, A.A. Serga and B. Hillebrands, Nat. Phys. **11**, 453-461 (2015).
[15] D. Grundler, Nat. Nanotech. **11**, 407-408 (2016).
[16] K. Wagner, A. Kákay, K. Schultheiss, A. Henschke, T. Sebastian and H. Schultheiss, Nat. Nanotech. **11**, 432-436 (2016).
[17] A. Khitun, M. Bao and K. L. Wang, J. Phys. D: Appl. Phys. **43**, 264005 (2010).
[18] H. Yu, O. Allivy Kelly, V. Cros, R. Bernard, P. Bortolotti, A. Anane, F. Brandl, F. Heimbach, and D. Grundler, Nat. Commun. **7**, 11255 (2016).
[19] T. Liu, H. Chang, V. Vlaminck, Y. Sun, M. Kabatek, A. Hoffmann, L. Deng and M. Wu, J. Appl. Phys. **115**, 87-90 (2014).
[20] H. Chang, P. Li, W. Zhang, T. Liu, A. Hoffmann, L. Deng and M. Wu, IEEE Magn. Lett. **5**, 6700 (2014).
[21] S. Urazhdin, V.E. Demidov, H. Ulrichs, T. Kendziorczyk, T. Kuhn, J. Leuthold, G. Wilde and S.O. Demokritov, Nat. Nanotech. **9**, 509-513 (2014).
[22] A. Haldar, D. Kumar and A.O. Adeyeye, Nat. Nanotech. **11**, 437-443 (2016).
[23] M. Krawczyk and D. Grundler, J. Phys.: Condens. Matter **26**, 126202 (2014).
[24] G. Gubbiotti, S. Tacchi, G. Carlotti, N. Singh, S. Goolaup, A.O. Adeyeye and M. Kostylev, Appl. Phys. Lett. **90**, 092503 (2007).
[25] Z.K. Wang, V.L. Zhang, H.S. Lim, S.C. Ng, M.H. Kuok, S. Jain and A.O. Adeyeye, ACSnano **4**, 643-648 (2010).
[26] A.V. Chumak, P. Pirro, A.A. Serga, M.P. Kostylev, R.L. Stamps, H. Schultheiss, K. Vogt, S.J. Hermsdoerfer, B. Laegel, P.A. Beck and B. Hillebrands, Appl. Phys. Lett. **95**, 262508 (2010).
[27] J. Topp, D. Heitmann, M.P. Kostylev and D. Grundler, Phys. Rev. Lett. **104**, 207205 (2010).
[28] J. Ding, M. Kostylev and A.O. Adeyeye, Appl. Phys. Lett. **100**, 073114 (2012).
[29] B. Obry, P. Pirro, T. Braecher, A.V. Chumak, J. Osten, F. Ciubotaru, A.A. Serga, J. Fassbender and B. Hillebrands, Appl. Phys. Lett. **104**, 042403 (2014).
[30] G.N. Kakazei, X.M. Liu and A.O. Adeyeye, Appl. Phys. Lett. **102**, 202403 (2014).
[31] A.V. Chumak, A.A. Serga and B. Hillebrands, Nat. Commun. **5**, 4700 (2014).
[32] A. Khitun and K.L. Wang, Superlatt. Microstruct. **38**, 184-200 (2005).
[33] See Supplemental Material for sample fabrication details and a full device image with integrated CPWs, more information about and the results of the simulations, the measurement technique, the full spectra of the Co/YIG sample, the coupling strength dependence on Co nanowire widths, and control measurements on samples with Al_2O_3 spacers, which includes Refs. [8, 34, 35, 44].
[34] W.S. Ament and G.T. Rado, Phys. Rev. **97**, 1558-1566 (1955).
[35] S. Klingler, A.V. Chumak, T. Mewes, B. Khodadadi, C. Mewes, C. Dubs, O. Surzhenko, B. Hillebrands and A. Conca, J. Phys. D **48**, 15001 (2015).
[36] V. Vlaminck and M. Bailleul, Science **322**, 410 (2008).
[37] S. Neusser, G. Durr, H.G. Bauer, S. Tacchi, M. Madami, G. Woltersdorf, G. Gubbiotti, C.H. Back and D. Grundler Phys. Rev. Lett. **105**, 067208 (2010).
[38] H. Yu, O. Allivy Kelly, V. Cros, R. Bernard, P. Bortolotti, A. Anane, F. Brandl, R. Huber, I. Stasinopoulos and D. Grundler Sci. Rep. **4**, 6848 (2014).
[39] S.J. Hamalainen, F. Brandl, K.J.A. Franke, D. Grundler and S. van Dijken, Phys. Rev. Appl. **8**, 014020 (2017).
[40] J. Ding, M. Kostylev and A.O. Adeyeye, Phys. Rev. B **84**, 054425 (2011).
[41] K.Y. Guslienko, S. O. Demokritov, B. Hillebrands and A. N. Slavin, Phys. Rev. B **66**, 132402 (2002).
[42] C. Kittel, Phys. Rev. **73**, 155 (1948).
[43] B. A. Kalinikos and A. N. Slavin *J. Phys. C: Solid State Phys.* **19**, 7013-7033 (1986).
[44] D.D. Stancil and A. Prabhakar, Spin Waves: Theory and Applications. Appendix C. *Springer* (2009).
[45] E.E. Shalyguina and K.-H. Shin, *J. Magn. Magn. Mater.* **220**, 167-174 (2000).

[46] C.S. Lin, H.S. Lim, Z.K. Wang, S.C. Ng and M.H. Kuok, *Appl. Phys. Lett.* **98**, 022504 (2011).
[47] B. Pigeau, C. Hahn, G. de Loubens, V.V. Naletov, O. Klein, K. Mitsuzuka, D. Lacour, M. Hehn, S. Andrieu and F. Montaigne, *Phys. Rev. Lett.* **109**, 247602 (2012).
[48] P. Hyde, L. Bai, D.M.J. Kumar, B.W. Southern, C.-M. Hu, S.Y. Huang, B.F. Miao and C.L. Chien, Phys. Rev. B **89**, 180404(R) (2014).
[49] C. Vittoria, Phys. Rev. B **37**, 2387 (1988).
[50] Y. Xiao, X.H. Yan, Y. Zhang, C. Liu, C.M. Hu, H. Guo, H. Yu and K. Xia, in preparation.
[51] Y.S. Chun and K.M. Krishnana, *J. Appl. Phys.* **95**, 6858 (2004).
[52] M. Pashkevich, A. Stupakiewicz, A. Kirilyuk, A. Maziewski, A. Stognij, N. Novitskii, A. Kimel and Th. Rasing *J. Appl. Phys.* **111**, 023913 (2012).
[53] N. Vukadinovic, J. Ben Youssef, V. Castel and M. Labrune, *Phys. Rev. B* **79**, 184405 (2009).
[54] J. Ben Youssef, V. Castel, N. Vukadinovic and M. Labrune, *J. Appl. Phys.* **108**, 063909 (2010).
[55] O. Dmytriiev, T. Meitzler, E. Bankowski, A. Slavin and V Tiberkevich, *J. Phys.: Condens. Matter* **22**, 136001 (2010).
[56] S. Klingler, V. Amin, S. Geprägs, K. Ganzhorn, H. Maier-Flaig, M. Althammer, H. Huebl, R. Gross, R.D. McMichael, M.D. Stiles, S.T.B. Goennenwein and M. Weiler, *Phys. Rev. Lett.* **120**, 127201 (2018).
[57] H. Qin, S.J. Hämäläinen and S. van Dijken, *Sci. Rep.* **8**, 5755 (2018).